Mechanical, Thermal, and Morphological Properties of Injection Molded Poly(lactic acid)/SEBS-*g*-MAH/Organo-Montmorillonite Nanocomposites

Y. Y. Leu, Z. A. Mohd Ishak, W. S. Chow

School of Materials and Mineral Resources Engineering, Engineering Campus, Universiti Sains Malaysia, Nibong Tebal 14300 Penang, Malaysia

Received 2 September 2010; accepted 13 June 2011
DOI 10.1002/app.35084
Published online 12 October 2011 in Wiley Online Library (wileyonlinelibrary.com).

ABSTRACT: Poly(lactic acid)/organo-montmorillonite (PLA/OMMT) nanocomposites toughened with maleated styrene-ethylene/butylene-styrene (SEBS-*g*-MAH) were prepared by melt-compounding using co-rotating twin-screw extruder followed by injection molding. The dispersibility and intercalation/exfoliation of OMMT in PLA was characterized using X-ray diffraction and transmission electron microscopy (TEM). The mechanical properties of the PLA nanocomposites was investigated by tensile and Izod impact tests. Thermogravimetric analyzer and differential scanning calorimeter were used to study the thermal behaviors of the nanocomposite. The homogenous dispersion of the OMMT silicate layers and SEBS-*g*-MAH encapsulated OMMT layered silicate can be observed from TEM. Impact strength and elongation at break of the PLA nanocomposites was enhanced significantly by the addition of SEBS-*g*-MAH. Thermal stability of the PLA/OMMT nanocomposites was improved in the presence of SEBS-*g*-MAH. © 2011 Wiley Periodicals, Inc. J Appl Polym Sci 124: 1200–1207, 2012

Key words: nanocomposites; organoclay; thermal properties; mechanical properties; morphology

INTRODUCTION

Organic/inorganic hybrid nanocomposites have received significant attentions from both academic and industrial sectors due to their excellent enhancement in certain physical and chemical properties compared with the pure material. The optimization of properties for the polymer/layered silicate nanocomposites are depending on several factors, for example, distribution and dispersion of the layered silicate in the polymer matrix, intercalation-, and exfoliation-ability of the layered silicate, compatibility between the polymer and layered silicate, and processability of the nanocomposites.

Poly(lactic acid) (PLA) synthesized from renewable resources has become popular owing to their sustainability, biodegradability, and superior transparency. These properties make it to be a potential material in the packaging, medical devices, and tissue engineering application.[1] Recently, many PLA-based nanocomposites, prepared by the addition of nanofillers such as organo-montmorillonite (OMMT), nanocalcium carbonate, titanium oxide nanoparticles, cellulose nanofiber, and carbon nanotube,[2–6] exhibited remarkable improvement in mechanical and thermal properties, dimensional stability, barrier, and physicochemical behaviors.

Although the hybridization of polymer and nanoclay can be a potential class of materials, the incompatibility between the two phases and the embrittlement of the resulting nanocomposites always the top priority issue. There are, at least two alternatives to improve the properties of polymer-clay nanocomposites, that is, functionalization of nanoclay and addition of polymeric compatibilizer. The exfoliation of silicate layers in low-density polyethylene was achieved by the incorporation of maleic anhydride grafted low-density polyethylene.[7] Impact strength and ductility of polyamide 6/polypropylene was improved significantly by the addition of maleic anhydride grafted styrene-ethylene/butylene-styrene copolymers (SEBS-*g*-MAH).[8,9] The flexural yield displacement of PLA/nanoclay nanocomposite was increased in the presence of maleic anhydride grafted ethylene propylene rubber (EPR-*g*-MAH).[10] Super-tough polyamide 6/OMMT nanocomposite was obtained with 30 wt % of maleinized styrene–ethylene/butylene–styrene copolymers.[11]

In addition, most of the nanoclay reinforced PLA nanocomposites demonstrated unsatisfied fracture toughness, impact strength and elongation at break.[12]

Correspondence to: W. S. Chow (shyang@eng.usm.my).

Contract grant sponsor: Universiti Sains Malaysia Research University (RU) Grant; contract grant number: 814070.

Contract grant sponsor: USM Incentive Grant; contract grant number: 8021013.

Contract grant sponsor: USM Postgraduate Research Grant Scheme; contract grant number: USM-RU-PGRS 8033002.

There are some approaches, which allowed to improve the toughness of the polymer-nanoclay nanocomposites, for example, plasticization by using rubber, addition of core-shell rubber particle and incorporation of toughening agent.[13] From the recent reports, maleated rubbers [e.g., maleic anhydride grafted styrene–ethylene/butylene–styrene copolymers (SEBS-*g*-MAH), maleic anhydride grafted ethylene propylene rubber (EPM-*g*-MAH)] served well in toughening the polymer-clay nanocomposites. From the literature, it was found that the incorporation of SEBS-*g*-MAH had improved the ductility and fracture toughness of the PA6/4% OMMT nanocomposite,[14] impact strength of polycarbonate/clay nanocomposites[15] and isotactic polypropylene/nano-magnesium hydroxide nanocomposites.[16]

In this research, we hypothesize that the thermal and impact properties of the Poly(lactic acid)/organo-montmorillonite (PLA/OMMT) nanocomposites can be improved by the addition of SEBS-*g*-MAH. The mechanical properties of the PLA nanocomposites will be correlated with its morphology (dispersibility and exfoliation-ability of nanoclay).

EXPERIMENTAL

Materials

PLA (Ingeo™ 3051D) was purchased from NatureWorks LLC® (Minnetonka, USA). The specific gravity and melt flow index of the PLA were 1.25 and 25 g/10 min (2.16 kg loads, 210°C), respectively. The glass transition temperature (T_g) and melting temperature (T_m) of the PLA are ~ 65 and 165°C, respectively. The organo-montmorillonite [OMMT, (Nanomer® I.30TC)] used in this study was a commercially available montmorillonite-layered silicate purchased from Nanocor (Nanocor, Aberdeen, USA). The OMMT composed of ~ 70% montmorillonite (MMT) intercalated by 30% octadecylamine. The cation exchange capacity and the aspect ratio of the OMMT were 120 meq/100 g and 300 – 500, respectively. The SEBS-*g*-MAH was purchased from Shanghai Jianqiao Plastic (Shanghai, China). The melt flow index and specific gravity of the SEBS-*g*-MAH were 1.0 g/10 min and of 0.91, respectively. The grafting content of MAH on SEBS is ~ 0.9 wt %. The materials designation and composition of PLA/OMMT nanocomposites is shown in Table I.

Preparation of PLA/OMMT nanocomposites

Prior to extrusion, PLA pellets and OMMT powders were dried at 80°C for 15 h in vacuum oven (Memmert GmbH, model VO500, Germany). The PLA, OMMT, and SEBS-*g*-MAH were pre-mixed by tumbling process. Then, the PLA/OMMT was melt-compounded using a corotating twin-screw extruder (Sino-Alloy Machinery, model PSM30, Taiwan). The temperature zone was set in the range of 160–190°C. The screw speed was set at 150 rpm. The PLA nanocomposites specimen was injection molded using an injection-molding machine (Haitian HTF86X1, Canada). The barrel temperatures were set at a range of 165–190°C, from the feeding section to the nozzle, respectively. Prior to injection molding, the PLA extrudates were dried in a vacuum oven at 80°C for 15 h.

TABLE I
Materials Designation, Composition, MFI of PLA, and PLA/OMMT Nanocomposites

Materials designation	Composition			MFI (g/10 min)
	PLA (wt %)	OMMT (wt %)	SEBS-*g*-MAH (phr)	
PLA	100	0	0	15.9
PLA/OMMT	98	2	0	13.2
PLA/OMMT/S5	98	2	5	13.2
PLA/OMMT/S10	98	2	10	10.3
PLA/OMMT/S15	98	2	15	8.1
PLA/OMMT/S20	98	2	20	6.9

Melt flow index (MFI) measurements

The measurement of melt flow index (MFI) was conducted using Dynisco Melt Flow Indexer (LMI4000), which adopted ASTM D1238 standard. The load and temperature was set at 2.16 kg and 190°C, respectively.

Transmission electron microscopy (TEM) and X-ray diffraction analysis

TEM measurements were carried out with a Ziess Libra 120 Plus energy filtering transmission electron microscope operating at an accelerating voltage of 120 kV. The specimens were prepared using a PT-PC PowerTome ultramicrotome (Boeckeler Instruments). Ultrathin sections of about 50 nm in thickness of the PLA nanocomposite specimen was cut with a Diatome diamond knife (45°) at room temperature. Then the specimen was stained with osmium tetroxide (OsO_4) for 1 h.

The intercalation of OMMT in the PLA nanocomposites was characterized by an X-ray diffractometer (XRD, Bruker AXS, model D8 Advance). The samples were scanned in fixed step size, 0.050 with a step-time of 0.1s in the range of 1° – 10°. The interlayer spacing of the OMMT was derived from the peak position (d_{001} − reflection) in the XRD diffractograms according to the Bragg's Equation [c.f. eq. (1)].

$$n\lambda = 2d \sin\theta \quad (1)$$

where the integer n referred to the degree of the diffraction, λ is the wavelength, d is the interlamellar spacing (d-spacing) and the experimental 2θ value is the angle between the diffracted and incoming X-ray waves.

Thermal analysis

The thermal stability and decomposition temperature of the PLA nanocomposites was characterized using

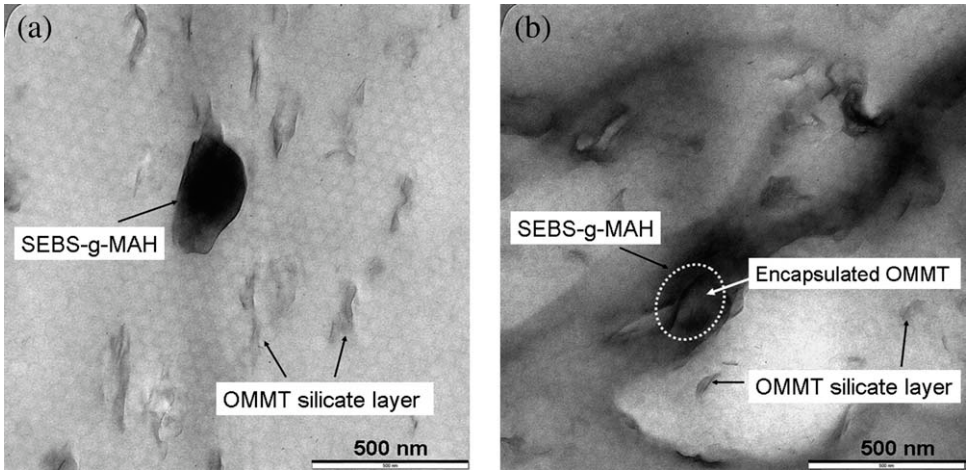

Figure 1 (a) TEM image of PLA/OMMT/S5 nanocomposites. (b) TEM image of PLA/OMMT/S20 nanocomposites.

thermogravimetric analyzer (TGA, Perkin Elmer, Pyris 6). The specimens were heated from room temperature to 600°C at a heating rate of 10°C/min in nitrogen atmosphere. Differential scanning calorimeter (DSC) (Perkin Elmer, DSC 6) was used to evaluate the thermal behavior of the PLA/OMMT nanocomposites. The specimens were scanned from 30 to 190°C at a heating rate of 10°C/min and held for 1 minute at 190°C. Then, they were cooled from 190 to 30°C at a cooling rate of 10°C/min and held for 1 minute at 30°C. Second scanning was performed similar to the first scanning in order to erase the thermal history. The glass transition temperature (T_g), melting temperature (T_m), and cold crystallization temperature (T_c) were determined. The degree of crystallinity (χ_c) of PLA nanocomposites was calculated using eq. (2):

$$\chi_c = [\Delta H_m/(\Delta H_f \times w_{\mathrm{PLA}})] \times 100\% \quad (2)$$

where χ_c is degree of crystallinity; ΔH_m is the heat of fusion of the sample; ΔH_f corresponds to the heat of fusion for 100% crystalline material, and w_{PLA} is the weight fraction of the PLA. The heat of fusion of 100% crystalline PLA (ΔH_f) is $\sim$ 93.6 J/g.[17]

For uncompatibilized PLA/OMMT nanocomposite sample, the w_{PLA} was calculated using eq. (3):

$$w_{\mathrm{PLA}} = 1 - w_{\mathrm{OMMT}} \quad (3)$$

where w_{OMMT} is the weight fraction of the OMMT.

For SEBS-*g*-MAH compatibilized PLA/OMMT nanocomposite samples, the w_{PLA} was calculated using eq. (4):

$$w_{\mathrm{PLA}} = 1 - w_{\mathrm{OMMT}} - w_{\mathrm{SEBS}-g-\mathrm{MAH}} \quad (4)$$

where $w_{\mathrm{SEBS}\text{-}g\text{-}\mathrm{MAH}}$ is the weight fraction of the SEBS-*g*-MAH.

Mechanical properties characterization

Tensile and flexural tests were performed according to the ASTM D638 and ASTM D790 using an Instron 3366. The tensile test was conducted at a crosshead speed of 5 mm/min. While, the flexural test was performed using three-points bending configuration at crosshead speed of 1.5 mm/min and support span length of 50 mm. Izod impact test was carried out according to ASTM D5941. A Zwick analogue Izod/Charpy Impact Tester (Germany) with a pendulum of 7.5 J was used to determine the impact strength of the PLA nanocomposites.

RESULTS AND DISCUSSION

Melt flow index (MFI)

Table I shows the MFI values for the PLA and PLA/OMMT nanocomposites. One can clearly see that the MFI of the PLA decreased by the addition of OMMT. These observations confirm that the OMMT filler influence and restrict the flowability of PLA. Note that the MFI of the PLA/OMMT nanocomposites was further decreased by the increasing content of SEBS-*g*-MAH. This can be associated to the elastomeric behavior of SEBS-*g*-MAH. Similar result was reported by Yew et al.[18] The viscosity of PLA/rice starch composites increased by the incorporation of epoxidized natural rubber. In opinion of the authors, the lower MFI values for the PLA/OMMT/SEBS-*g*-MAH nanocomposites can be also explained by considering the interaction and affinity between the PLA, OMMT, and SEBS-*g*-MAH, which might restrict the chains mobility and led to higher viscosity. Therefore, the processability of PLA/OMMT nanocomposites decreased marginally with the increase of SEBS-*g*-MAH content.

Morphology of nanocomposites

Figure 1(a,b) show the TEM images taken from the PLA/OMMT/S5 and PLA/OMMT/S20 nanocomposite respectively. The dark gray lines represented the thickness of individual clay layer or their tactoids. One may observe that the dispersibility of the

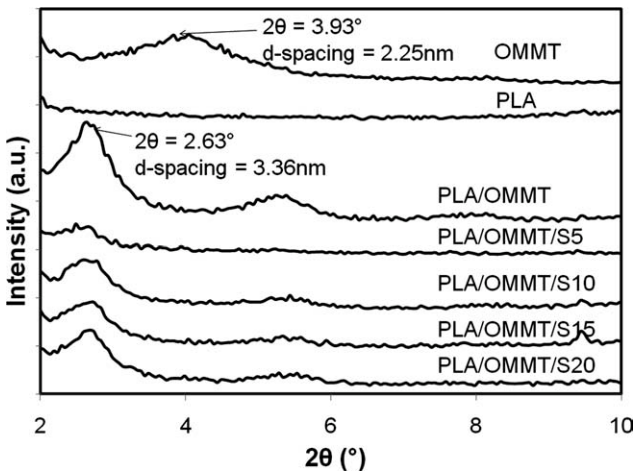

Figure 2 XRD patterns of OMMT, PLA, and PLA/OMMT nanocomposites.

OMMT layered silicate in the PLA is quite well and homogeneous. From the TEM micrograph, intercalated and exfoliated OMMT were detected. The darker region can be ascribed to the SEBS-*g*-MAH. When treated with OsO_4, the butylene in SEBS-*g*-MAH will react preferentially and absorbed the oxide, and subsequently, stained in darker color. One can recognize that some of the OMMT layered silicate was encapsulated by SEBS-*g*-MAH [c.f. Fig. 1(b)]. This is probably due to the high affinity of the maleic anhydride groups in SEBS-*g*-MAH with the OMMT.[19] The XRD diffratograms of OMMT and PLA nanocomposites are shown in Figure 2. OMMT exhibited a characteristic peak at $2\theta = 3.93°$, which corresponding to a basal spacing of 2.25 nm. Intercalated PLA/OMMT nanocomposites were obtained, as indicated by the shifting of the 2θ to a lower angle (i.e., $\approx 2.63°$) and the increasing of the *d*-spacing to 3.36 nm.

Thermal analysis

The TGA curves of OMMT, PLA, SEBS-*g*-MAH, and PLA nanocomposites are displayed in Figure 3(a). Figure 3(b) shows the DTG curves of the materials investigated. The TGA results (e.g., T_{95}, T_{50}, T_{d1}, and T_{d2}) of PLA and its nanocomposites are tabulated in Table II. It can be seen that the decomposition of OMMT started at 350°C and with a total mass loss of 25.2%. This is associated to the decomposition of organic intercalant of the OMMT (i.e., octadecylamine). At 600°C, ~ 72.7% of the residue ash remained, which can be attributed to the montmorillonite (MMT) content. T_{95} and T_{50} referred to the temperature at which the remaining mass of the materials is 95 and 50%, respectively. The first and second stage decomposition temperatures referred to T_{d1} and T_{d2}, respectively. The T_{d1} in the range of 353–367°C is related to the thermal dissociation of the PLA macromolecule chains while the T_{d2} in the range of 451–460°C is associated to the thermal degradation of SEBS-*g*-MAH. Based on TGA curves in Figure 3(a), one can observe that the onset of decomposition temperature for SEBS-*g*-MAH is started at ~ 440°C. According to Chow and Neoh,[15] the decomposition of SEBS-*g*-MAH fell in the range of 425–465°C. The PLA/OMMT nanocomposite exhibited lower T_{95}, T_{50}, and T_{d1} values compared with that of pure PLA. This is due to the decomposition of organic intercalant of the OMMT and subsequently accelerated the thermal degradation of PLA.[10] However, both T_{95} and T_{50} values, as well as the T_{d1} of the PLA/OMMT nanocomposite increased significantly with the addition of SEBS-*g*-MAH. This indicates that the incorporation of SEBS-*g*-MAH increased the thermal stability of the PLA/OMMT nanocomposites. This was accompanied with the shifting of decomposition temperature towards higher values. Moreover, thermal stability of the PLA/OMMT nanocomposites improved notably as

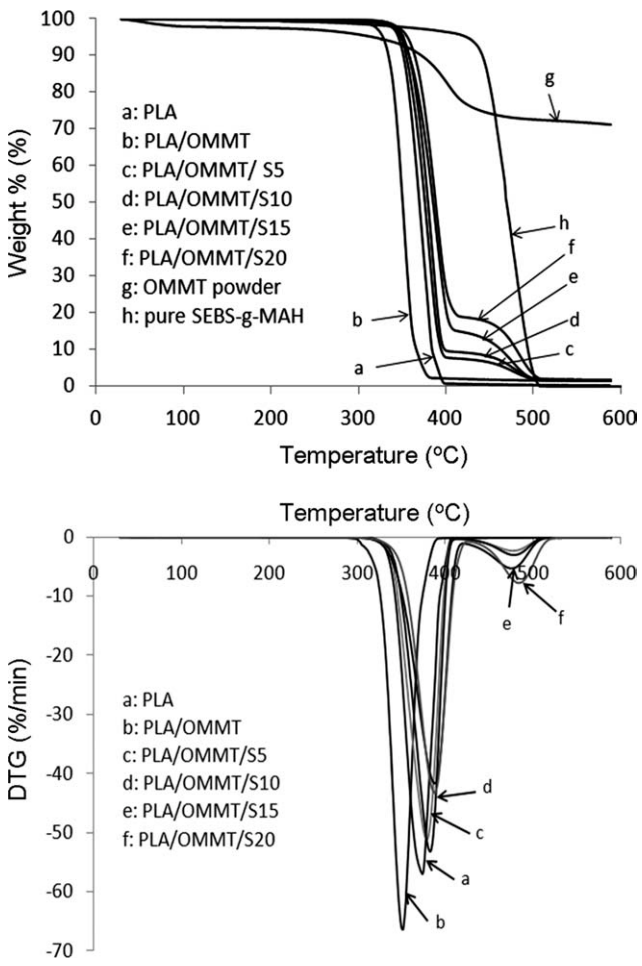

Figure 3 (a) TGA curves of OMMT, SEBS-*g*-MAH, PLA, and PLA/OMMT nanocomposites. (b) DTG curves of PLA and PLA/OMMT nanocomposites.

TABLE II
TGA Data of PLA and PLA/OMMT Nanocomposites

Materials designation	T_{95} (°C)	T_{50} (°C)	T_{d1} (°C)	T_{d2} (°C)
PLA	346.0	370.1	353.4	–
PLA/OMMT	328.4	350.4	336.3	–
PLA/OMMT/S5	348.6	375.6	356.6	451.6
PLA/OMMT/S10	351.2	379.3	360.4	455.3
PLA/OMMT/S15	348.4	385.2	363.6	454.6
PLA/OMMT/S20	356.2	388.2	367.4	460.8

the increasing content of SEBS-*g*-MAH. A possible reason of this observation should be related to the thermal stable styrene in SEBS-*g*-MAH. In addition, SEBS-*g*-MAH can provide a large physical protective barrier of OMMT on the surface for the PLA matrix, which further restricts the diffusion of volatile decomposition products within the nanocomposites.

The DSC thermograms of PLA and its nanocomposites are shown in Figure 4. The thermal characteristics (e.g., T_g, T_c, and T_m) of the PLA nanocomposites are summarized in Table III. The glass transition temperatures (T_g) of the PLA and PLA/OMMT nanocomposites were almost similar, which is approximately 61°C. This indicates that the T_g of PLA is practically unaltered by the addition of OMMT and SEBS-*g*-MAH. Apparently, one may recognize that the cold crystallization temperature of PLA was decreased by the incorporation of OMMT. This is attributed to the larger surface areas and volume ratios of the OMMT particulates, which gave rise to more nucleating sites and led to enhanced cold crystallization ability in PLA.[10] However, the cold crystallization temperature of PLA/OMMT nanocomposites was increased about 13°C by the addition of SEBS-*g*-MAH. This is probably due to the encapsulation of OMMT by SEBS-*g*-MAH, which subsequently retarded the nucleating effect of OMMT.

The effects of OMMT and SEBS-*g*-MAH on the degree of crystallinity (χ_c) for PLA are highlighted in Table III. It can be clearly seen that the χ_c of PLA was marginally reduced by the addition of OMMT. This can be associated to the higher interfacial area and adhesion between the PLA matrix and intercalated/exfoliated OMMT, which can act to reduce the

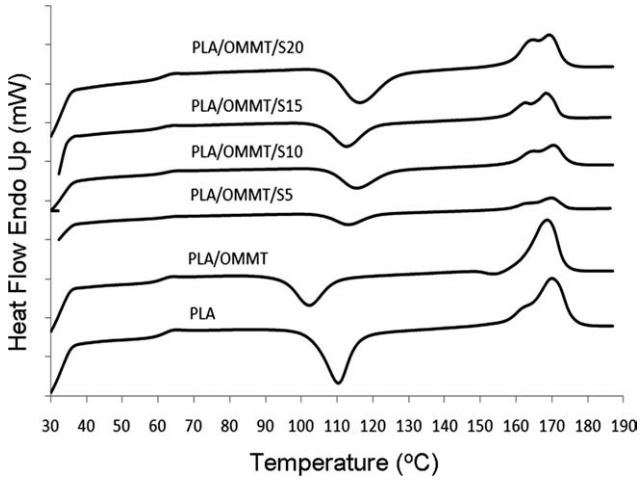

Figure 4 DSC thermograms of PLA and PLA/OMMT nanocomposites.

mobility of crystallizable chain segments. The physical hindrance of OMMT layers hindered the motions of the macromolecular chains of PLA to align during the crystallization process. Similar observation was reported by Gopakumar et al.[20] on the thermo-crystallization of polyethylene/montmorillonite composites. From Table III, it can be observed that the χ_c of PLA/OMMT nanocomposites decreased noticeably in the presence of 5 phr SEBS-*g*-MAH, but increased gradually with further loading of SEBS-*g*-MAH (10–20 phr). This suggests that the presence of higher concentration of SEBS-*g*-MAH favored the crystallization of the PLA.

In Figure 4, PLA displayed a melting temperature peak (T_α) at 170°C with a shoulder peak ($T_{\alpha'}$) at 162.1°C. This bimodal melting peak was induced when the less perfect crystals have enough time to melt and reorganize into crystals with higher structural perfection, and later remelt at higher temperature.[21] PLA can crystallize in several polymorphic forms, that is, α, β, and γ forms, depending on the preparation conditions.[22] A double melting endotherm was often observed in PLA and depending on the crystallization temperature.[23] The two crystal modifications that could grow upon melt crystallization are the α-form, that predominated at high crystallization temperatures, and the α′-form that grew

TABLE III
DSC Thermal Characteristics of PLA and PLA/OMMT Nanocomposites

	Thermal Characteristics						
Materials designation	T_g (°C)	T_c (°C)	$T_{\alpha'}$ (°C)	T_α (°C)	ΔH_c (J/g)	ΔH_m (J/g)	χ_c (%)
PLA	61.8	110.2	162.1	170.0	27.3	31.2	33.3
PLA/OMMT	60.8	102.1	–	168.7	19.5	28.8	31.4
PLA/OMMT/S5	61.9	113.1	163.2	169.7	14.7	15.7	18.0
PLA/OMMT/S10	60.7	114.3	162.2	168.9	16.9	16.9	20.2
PLA/OMMT/S15	60.7	112.6	162.4	168.7	22.1	23.5	29.4
PLA/OMMT/S20	61.5	116.3	162.8	169.1	26.1	25.3	33.0

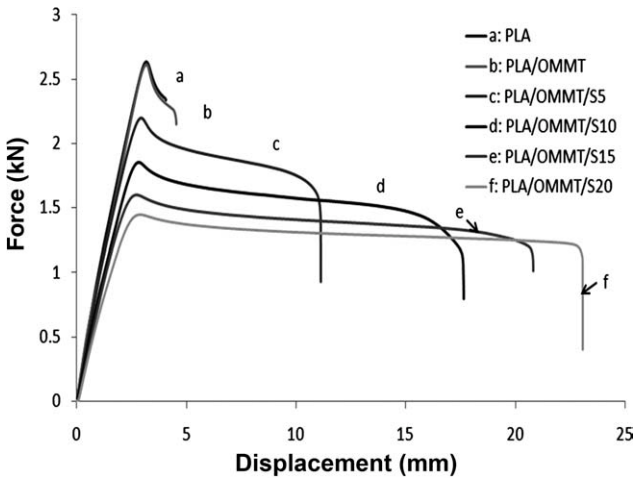

Figure 5 Typical force-displacement curves of the PLA and PLA/OMMT nanocomposites.

at low crystallization temperatures.[24,25] From Figure 4, an endothermic shoulder peak prior to the dominant melting peak in the DSC heating curve of PLA/OMMT nanocomposite was detected. Note that the shoulder peak ($T_{\alpha'}$) of the PLA was disappeared in the presence of OMMT. According to Pan et al.,[24] the α′-to-α transition mainly involved slight rearrangement of the molecular packing within the unit cell to the more energy-favorable state, corresponding to a reduction of lattice dimensions. The α′-to-α transformation mainly proceeded by a direct solid-solid transition mechanism which resulted only a single melting peak with an endothermic shoulder peak. Day et al.[26] reported that the presence of the OMMT appeared to be influencing the nucleation and crystal growth rate of the PLA.

Based on DSC thermograms in Figure 4, one may observe that the bimodal melting peak reappeared for PLA/OMMT nanocomposites with the addition of SEBS-*g*-MAH. With the increase in crystallization temperature, the melting of PLA changes from a polymorphic phase transition to the melt-recrystallization mechanism, and thus two endothermic peaks are observable. This may suggests that the OMMT reduced the T_c of PLA system and induced polymorphic phase transition mechanism. However, encapsulation of OMMT by SEBS-*g*-MAH retarded the PLA cold crystallization ability and led to an increase on the T_c of the materials. Therefore, melt-recrystallization mechanism is again being observed in the DSC melting thermograms of PLA/OMMT/SEBS-*g*-MAH nanocomposites.

Mechanical properties

Figure 5 shows the typical force-displacement curves of the PLA and PLA/OMMT nanocomposites with and without SEBS-*g*-MAH. It can be seen that the PLA and PLA/OMMT nanocomposite demonstrated brittle behaviors. Neat PLA fractured without necking indicating a brittle fracture. However, PLA/OMMT/SEBS-*g*-MAH nanocomposites experienced significant plastic deformation and necking compared with that of PLA and PLA/OMMT nanocomposite. The mechanical properties of PLA and its nanocomposites are tabulated in Table IV. The tensile modulus of PLA increased significantly by the addition of OMMT. This is attributed to the rigidity and reinforcing-ability of the OMMT. However, the incorporation of SEBS-*g*-MAH decreased the tensile modulus of PLA/OMMT nanocomposites. This is associated to the lower modulus and elastomeric nature of SEBS-*g*-MAH. Similar observation was reported by Kusmono et al.[8] on the PA6/PP/SEBS-*g*-MAH/OMMT and González[11] on the PA6/SEBS-*g*-MAH/OMMT nanocomposites. Note that the tensile strength of PLA and PLA/OMMT nanocomposites is still comparable. On the contrary, the tensile strength of the PLA/OMMT nanocomposites decreased marginally with the increasing content of SEBS-*g*-MAH. This is again related to the elastomeric nature of the SEBS-*g*-MAH. Note that the tensile strength of SEBS-*g*-MAH is ~ 34.5 MPa, which is much lower than that of PLA. Thus, it is not a

TABLE IV
Mechanical Properties of PLA and PLA/OMMT Nanocomposites

	Materials designation					
Mechanical Properties	PLA	PLA/ OMMT	PLA/ OMMT/S5	PLA/OMMT/ S10	PLA/OMMT/ S15	PLA/OMMT/ S20
Tensile Modulus (GPa)	1.2 (± 0.020)	1.3 (± 0.016)	1.1 (± 0.036)	1.1 (± 0.008)	1.0 (± 0.022)	0.9 (± 0.028)
Tensile Strength (MPa)	59.4 (± 0.43)	58.7 (± 0.30)	48.8 (± 0.29)	42.3 (± 0.78)	37.1 (± 0.17)	33.7 (± 0.37)
Elongation at break (%)	8.4 (± 0.16)	10.4 (± 2.31)	21.7 (± 1.36)	32.6 (± 3.24)	41.6 (± 2.59)	46.4 (± 3.78)
Flexural Modulus (GPa)	3.6 (± 0.072)	4.0 (± 0.053)	3.4 (± 0.073)	3.3 (± 0.069)	3.0 (± 0.059)	2.7 (± 0.030)
Flexural Strength (MPa)	97.0 (± 0.24)	97.8 (± 0.87)	76.5 (± 0.80)	71.1 (± 0.68)	65.0 (± 0.37)	58.1 (± 1.24)
Izod Impact Strength (kJ/m^2) [Unnotched]	23.1 (± 2.07) [control]	19.8 (± 2.54) [−14.3%]	46.9 (± 5.17) [+136.9%]	53.4 (± 4.94) [+169.7%]	74.5 (± 1.87) [+276.3%]	Nonbreak
Izod Impact Strength (kJ/m^2) [Notched]	6.9 (± 2.28) [control]	3.6 (± 0.07) [−47.8%]	7.24 (± 1.78) [+101.1%]	8.9 (± 0.74) [+147.2%]	9.3 (± 1.4) [+158.3%]	11.2 (± 2.11) [+211.1%]

surprise that higher content of SEBS-*g*-MAH would remarkably reduce the tensile strength of PLA/OMMT nanocomposites. From Table IV, it can be seen that the elongation at break of the PLA did not scarified by the addition of OMMT. According to Wnek and Bowlin,[27] the polar functional groups presented in the PLA created strong interchain secondary bonds. Hence, the polymers chains could not slip pass each other when the tensile force was applied. Therefore, neat PLA has low elongation at break. The addition of OMMT in PLA matrix reduced the PLA interchain secondary bonds, led to the occurrence of shear yielding by exhibiting intense stress whitening at the fracture surface during the tensile deformation, and followed by necking. Note that the elongation at break of PLA/OMMT nanocomposites increased gradually as the increasing content of SEBS-*g*-MAH. This is because SEBS-*g*-MAH can act as stress concentrator and absorb a high amount of energy during the tensile deformation. Moreover, in opinion of the authors some of the OMMT layered silicates are encapsulated by the SEBS-*g*-MAH. Therefore, the nanocomposites might elongate largely avoiding a highly localized strain process.[28] The flexural modulus and strength of PLA and its nanocomposites are also listed in Table IV. The addition of OMMT in PLA remarkably increased its flexural modulus and strength. These improvements could be attributed to high stiffness and high aspect ratio of OMMT, which led to better exfoliation and reinforcing-ability in the PLA system. On the contrary, the presence of SEBS-*g*-MAH decreased the flexural modulus and strength of the PLA/OMMT nanocomposites and the effect became prominent as the loading of SEBS-*g*-MAH increased. The phenomenon was again attributed to the elastomeric nature of SEBS-*g*-MAH.

As shown in Table IV, the PLA/OMMT nanocomposites exhibited lower impact strength compared to that of neat PLA (both notched and un-notched samples). This is probably due to the heterogeneous structure of the PLA/OMMT nanocomposites. Moreover, clusters of OMMT particle might appear and acted as stress concentration sites, triggered brittle response, and material failure in the impact testing.[3] As expected, the impact strength of the PLA/OMMT increased significantly by the addition of SEBS-*g*-MAH. The toughening effect was further increased as the SEBS-*g*-MAH content increased. The enhancement of impact strength of the PLA/OMMT/SEBS-*g*-MAH nanocomposites could be related to the homogeneous dispersion and distribution of SEBS-*g*-MAH small domains in the PLA matrix. The elastomeric characteristic of SEBS-*g*-MAH enabled to absorb impact energy and acted as a stress concentrator during the impact deformation. The SEBS-*g*-MAH elastomeric component can induced energy dissipation mechanisms in PLA, which retarded crack initiation and propagation, and subsequently led to better toughness improvement. Note that the percentage of improvement in impact strength of notched PLA nanocomposites was relatively lower than that of un-notched counterparts (c.f. Table IV). Since PLA is classified as brittle materials, they were quite sensitive to notches and local nonhomogeneities. Even though the addition of SEBS-*g*-MAH increased the absorbed impact energy ability of the nanocomposites, the notches still facilitated failure under impact conditions due to localized stress concentrations.

CONCLUSIONS

Based on this work devoted to study the effect of SEBS-*g*-MAH on the properties of the PLA/OMMT nanocomposites, the following conclusions can be drawn.

A mixture of intercalated and exfoliated structure of OMMT coexist in the PLA matrix, while, in some case, encapsulation of OMMT by SEBS-*g*-MAH did occurred. The thermal behavior (especially crystallization temperature and degree of crystallinity–as detected from DSC) of PLA was greatly influenced by the addition of OMMT and SEBS-*g*-MAH. TGA results revealed that the thermal stability of PLA/OMMT nanocomposites increased profoundly by the addition of SEBS-*g*-MAH. In this work, SEBS-*g*-MAH can act as a good toughening agent for PLA/OMMT nanocomposites. This is reflected in improved elongation at break and impact strength, however, at cost of modulus and strength. Overall, the PLA/OMMT/SEBS-*g*-MAH (5 phr) exhibited a balance in processability, mechanical, and thermal properties.

The authors appreciate the technical assistance from Unicolour Polymer Technology Sdn Bhd (Malaysia).

References

1. Auras, R. A.; Lim, L. T.; Selke, S. E. M.; Tsuji, H. Poly(lactic acid): Synthesis, Structures, Properties, Processing and Applications; Wiley: New Jersey, 2010.
2. Zhou, Q.; Xanthos, M. Polym Degrad Stab 2008, 93, 1450.
3. Long, J.; Zhang, J. W.; Wolcott, M. P. Polymer 2007, 48, 7632.
4. Chen, C. C; Gang, L. V.; Pan, C.; Song, M.; Wu., C. H.; Guo, D. D.; Wang, X. M.; Chen, B. A.; Gu, Z. Z. Biomed Mater 2007, 2, L1.
5. Iwatake, A.; Nogi, M.; Yano, H. Compos Sci Technol 2008, 68, 2103.
6. Hapuarachchi, T. D.; Peijs T. Compos Part A Appl Sci Manuf 2010, 41, 954.
7. Morawiec, J.; Pawlak, A.; Slouf, M.; Galeski, A.; Piorkowska, E.; Krasnikowa, N. Eur Polym J 2005, 41, 1115.
8. Kusmono; Mohd Ishak, Z. A.; Chow, W. S.; Takeichi, T.; Rochmadi. Eur Polym J 2008, 44, 1023.

9. Kusmono; Mohd Ishak, Z. A.; Chow, W. S.; Takeichi, T.; Rochmadi. Compos A 2008, 39, 1802.
10. Chow, W. S.; Lok, S. K. J Therm Anal Calorim 2009, 95, 627.
11. González, I.; Eguiazábal, J. I.; Nazábal, J. Compos Sci Technol 2006, 66, 1833.
12. Rasal R. M.; Hirt, D. E. J Biomed Mater Res A 2008, 88A, 1079.
13. Argon, A. S.; Cohen, R. E. Polymer 2003, 44, 6013.
14. Tjong, S. C.; Bao, S. P.; Liang, G. D. J Polym Sci Part B: Polym Phys 2005, 43, 3112.
15. Chow, W. S.; Neoh, S. S. J Polym Plast Technol Eng 2010, 49, 62.
16. Liu, S. P.; Ying, J. R.; Zhou, X. P.; Xie, X. L.; Mai, Y. M. Compos Sci Technol 2009, 69, 1873.
17. Wang, H.; Sun, X. S.; Seib, P. J Appl Polym Sci 2001, 82, 1761.
18. Yew, G. H.; Mohd Yusof, A. M.; Mohd Ishak, Z. A.; Ishiaku, U. S. Polym Degrad Stab 2005, 90, 488.
19. Ahmadi, S. J.; Yu, D. H.; Wei, L. J Compos Mater 2004, 39, 745.
20. Gopakumar, T. G.; Lee, J. A.; Kontopoulou, M.; Parent, J. S. Polymer 2002, 43, 5483.
21. Sarasua, J. R.; Prud'homme, R. E.; Wisniewski, M.; Borgne, A. L.; Spassky, N. Macromolecules 1998, 31, 3895.
22. Calafel, M. I.; Remiro, P. M.; Cortázar, M. M.; Calahorra, M. E. Colloid Polym Sci 2009, 288, 28.
23. Di Lorenzo, M. L. J Appl Polym Sci 2006, 100, 3145.
24. Pan, P.; Kai, W.; Zhu, B.; Dong, T.; Inoue, Y. Macromolecules 2007, 40, 6898.
25. Pan, P.; Inoue, Y. Prog Polym Sci 2009, 34, 605.
26. Day, M.; Nawaby, A. V.; Liao, X. J Therm Anal Calorim 2006, 86, 623.
27. Wnek, G. E.; Bowlin, G. L. Encyclopedia of Biomaterials and Biomedical Engineering; Informa Health Care: New York, 2004.
28. Contreras, V.; Cafiero, M.; Silva, S. D.; Rosales, C.; Perera, R.; Matos, M. Polym Eng Sci 2006;46, 1111.